ORIGINAL PAPER

Modified torsion coefficients for a 3-D brick Cosserat point element

M. Jabareen · M. B. Rubin

Abstract A simple deformation field associated with an exact torsion-like solution of the equilibrium equations of linear elasticity is shown to provide a good approximation of the deformation field in interior elements of a mesh that models pure torsion of a right cylindrical bar with rectangular cross-section. Using this solution, modified torsion coefficients are proposed for a 3-D brick Cosserat point element (CPE) which are shown to improve convergence properties for solutions of pure torsion.

1 Introduction

Torsion of a right cylindrical region with arbitrary cross-section is a classical problem in the linear theory of elasticity. The exact solution for a rectangular cross-section with an isotropic material can be found in numerous texts (e.g., [22]) and for an orthotropic material can be found in [9].

Recently, Nadler and Rubin [11] have developed a 3-D eight noded brick Cosserat Point Element (referred to as CPE) which is based on the theory of a Cosserat point [14–17]. It has been shown [3,6–8,10,18] that the CPE is a robust user friendly element that can be used with confidence to

M. Jabareen (✉)
Institute of Mechanical Systems,
Department of Mechanical Engineering,
ETH Zentrum, 8092 Zurich, Switzerland
e-mail: mahmood.jabareen@imes.mavt.ethz.ch

M. B. Rubin
Faculty of Mechanical Engineering Technion,
Israel Institute of Technology, 32000 Haifa, Israel
e-mail: mbrubin@tx.technion.ac.il

model problems in nonlinear elasticity, including shells, plates and beams. In contrast with standard finite element methods the Cosserat approach treats the CPE as a structure whose response is characterized by a strain energy function. The constitutive coefficients in this strain energy function are determined by matching exact linear elastic solutions and no integration is needed over the element region.

In [11] the torsional constitutive coefficients for the CPE were determined by matching exact solutions for pure torsion of a rectangular parallelepiped. Since the strain and stress fields do not depend on the coordinate parallel to the torsion direction it is possible to use a mesh $\{n_1 \times n_2 \times 1\}$ with only one element in the torsion direction. If $n_1 = n_2 = 1$ and the rectangular parallelepiped is modeled by a single element then the lateral surfaces of the element are traction free and the element responds to pure torsion. However, when the mesh is refined (with $n_1 > 1$ and $n_2 > 1$) then a typical interior element no longer experiences pure torsion since its lateral surfaces are subjected to nonzero tractions.

It will be shown in this paper that the displacement field of a simple exact torsion-like solution of the equations of isotropic linear elasticity is representative of the deformation field in a typical interior element in a refined mesh for pure torsion. Modified torsional coefficients of the CPE are proposed which capture this simple solution and significantly improve the convergence properties of the CPE for pure torsion, while retaining the other good properties of the CPE for bending dominated fields and large deformations.

An outline of this paper is as follows. Section 2 reviews the classical solution for pure bending and introduces an exact simple torsion-like solution which is representative of the state in an interior element and which forms the basis for the modified torsional coefficients of the CPE that are proposed in Sect. 3. Section 4 presents example problems of small deformation pure torsion of a bar with a rectangular

cross-section and large deformation lateral torsional buckling of a cantilever beam. Then, conclusions are summarized in Sect. 5.

2 Summary of the exact pure torsion and torsion-like solutions

Here attention is limited to the simple case of an isotropic material and a bar which is a rectangular parallelepiped that is subjected to torsion. Specifically, the position vector $\mathbf{X}^*$ of a material point in the reference configuration is expressed in terms of its components X_i ($i = 1, 2, 3$) relative to fixed rectangular Cartesian base vectors $\mathbf{e}_i$ and the bar occupies the region

$$\mathbf{X}^* = \sum_{i=1}^{3} X_i \mathbf{e}_i, |X_1| \le \frac{L_1}{2}, |X_2| \le \frac{L_2}{2}, 0 \le X_3 \le L_{\frac{3}{2}}, \quad (1)$$

where L_i are lengths of the bar.

For the exact linear solution of pure torsion of the bar the displacement field can be expressed in the form (e.g., [22])

$$
\begin{aligned}
\mathbf{u}^* = &[\omega_1 \hat{\phi}_1^*(X_2, X_3) + \omega_2 X_2 X_3 - \omega_3 X_2 X_3]\mathbf{e}_1 \\
&+[-\omega_1 X_1 X_3 + \omega_2 \hat{\phi}_2^*(X_1, X_3) + \omega_3 X_1 X_3]\mathbf{e}_2 \\
&+[\omega_1 X_1 X_2 - \omega_2 X_1 X_2 + \omega_3 \hat{\phi}_3^*(X_1, X_2)]\mathbf{e}_3, \quad (2)
\end{aligned}
$$

where ω_i denote the constant twists per unit length in the $\mathbf{e}_i$ directions, respectively, and $\hat{\phi}_i^*$ are functions that control warping of the $X_i = $ constant cross-sections, respectively. The warping functions $\hat{\phi}_i^*$ are determined by satisfying equations of equilibrium (in the absence of body force) and boundary conditions on the lateral surfaces of the bar. Then, the exact solutions for the torsional stiffnesses B_i^* associated with pure torsional solutions are given by (e.g., [11,22]) in the forms

$$
\begin{aligned}
B_1^* &= \frac{T_1}{\omega_1} = \frac{\mu^* L_2^2 L_3^2}{3} b^* \left(\frac{L_2}{L_3}\right), \\
B_2^* &= \frac{T_2}{\omega_2} = \frac{\mu^* L_1^2 L_3^2}{3} b^* \left(\frac{L_1}{L_3}\right), \quad (3)\\
B_3^* &= \frac{T_3}{\omega_3} = \frac{\mu^* L_1^2 L_2^2}{3} b^* \left(\frac{L_1}{L_2}\right),
\end{aligned}
$$

where T_i is the torque caused by the twist ω_i, μ^* is the shear modulus and $b^*(\xi)$ is a function defined by

$$
\begin{aligned}
b^*(\xi) = \xi \left[1 - \frac{192}{\pi^5}\xi \sum_{n=1}^{\infty} \frac{1}{(2n-1)^5} \tanh\left\{\frac{\pi(2n-1)}{2\xi}\right\}\right]\\
\text{for } \xi \le 1, \quad (4)
\end{aligned}
$$

where use is made of the fact that

$$b^*(\xi) = b^*\left(\frac{1}{\xi}\right), \quad (5)$$

and that the series in (4) converges faster than series for $b^*(1/\xi)$ for $\xi \le 1$.

For a numerical solution of the problem of pure torsion with only one torque T_3 applied in the $\mathbf{e}_3$ direction, it is possible to consider an element mesh $\{n_1 \times n_2 \times 1\}$ with n_1 elements in the $\mathbf{e}_1$ direction, n_2 elements in the $\mathbf{e}_2$ direction and only one element in the $\mathbf{e}_3$ direction since there is no dependence of the strain and stress fields on the axial coordinate X_3. Then, the lengths H_i of these elements are given by

$$H_1 = \frac{L_1}{n_1}, \quad H_2 = \frac{L_2}{n_2}, \quad H_3 = L_3. \quad (6)$$

2.1 A simple exact torsion-like solution

As mentioned in the introduction, since the stress field for pure torsion associated with (2) varies over the cross-section, a typical element whose center is located by

$$\mathbf{X}^* = \bar{\mathbf{X}}^* = \sum_{i=1}^{3} \bar{X}_i \mathbf{e}_i, \quad (7)$$

is subjected to nonzero tractions on its lateral surfaces. Therefore, the displacement, strain and stress fields in a typical element associated the problem (2) cannot be locally approximated by pure torsion. Instead, the state in an interior element is more closely represented by a simpler exact torsion-like solution for which the displacement, strain and stress fields are specified by

$$
\begin{aligned}
\mathbf{u}^* = &(\omega_1 \Phi_1 + \omega_2 - \omega_3) X_2 X_3 \mathbf{e}_1 \\
&+(-\omega_1 + \omega_2 \Phi_2 + \omega_3) X_1 X_3 \mathbf{e}_2 \\
&+(\omega_1 - \omega_2 + \omega_3 \Phi_3) X_1 X_2 \mathbf{e}_3, \\
2\mathbf{E}^* = &[-\omega_1(1 - \Phi_1) + \omega_2(1 + \Phi_2)] X_3(\mathbf{e}_1 \otimes \mathbf{e}_2 + \mathbf{e}_2 \otimes \mathbf{e}_1) \\
&+[\omega_1(1 + \Phi_1) - \omega_3(1 - \Phi_3)] X_2(\mathbf{e}_1 \otimes \mathbf{e}_3 + \mathbf{e}_3 \otimes \mathbf{e}_1) \\
&+[-\omega_2(1 - \Phi_2) + \omega_3(1 + \Phi_3)] \\
&\quad X_1(\mathbf{e}_2 \otimes \mathbf{e}_3 + \mathbf{e}_3 \otimes \mathbf{e}_2), \mathbf{T}^* = 2\mu^* \mathbf{E}^*. \quad (8)
\end{aligned}
$$

where the constants Φ_i control the local warping fields. It can easily be seen that this stress field also satisfies the equations of equilibrium in the absence of body force. In the next section this simple torsion solution will be used to develop modified forms for the constitutive coefficients that control torsion in the CPE.

3 Relevant aspects of the CPE formulation

Recently, Nadler and Rubin [11] used the theory of a Cosserat point [14,15,17] to develop a new 3-D brick CPE for the numerical solution of problems in nonlinear elasticity. Within the context of this approach, the CPE is considered to be a

structure and the constitutive equations of the structure are specified in terms of a strain energy function Σ. Using a nonlinear form of the patch test, Nadler and Rubin [11] proposed a form for Σ which is determined by the strain energy function Σ^* of the 3-D material and a strain energy function Ψ for inhomogeneous deformations, such that

$$\Sigma = \Sigma^* + \Psi. \tag{9}$$

Following the work in [7] it is convenient to express Ψ in the form

$$2m\Psi = \frac{D^{1/2}V\mu^*}{6(1-\nu^*)}\left[\sum_{i=1}^{9}\sum_{j=1}^{9}B_{ij}b_ib_j\right] + D^{1/2}V[K_{16}(\kappa_4^1)^2 + K_{17}(\kappa_4^2)^2 + K_{18}(\kappa_4^3)^2], \quad B_{ij} = B_{ji}, \tag{10}$$

where m is the mass of the element, ν^* is Poisson's ratio, κ_j^i are strains due to inhomogeneous deformations, $D^{1/2}V$ is defined by the reference geometry of the element, $\{B_{ij}, K_{16}, K_{17}, K_{18}\}$ are constitutive constants and the auxiliary vector b_i is defined by

$$b_i = \{\kappa_1^1, \kappa_3^3, \kappa_1^2, \kappa_2^3, \kappa_2^1, \kappa_3^2, \kappa_1^3, \kappa_2^2, \kappa_3^1\}. \tag{11}$$

In [11] the constitutive constants associated with B_{ij} were determined by comparing solutions of the linearized CPE with exact solutions of a rectangular parallelepiped. For such an element the responses to bending, torsion and higher-order hourglassing are uncoupled ($B_{7i} = B_{8i} = B_{9i} = 0, i = 1, 2, \ldots, 6$). Specifically, in [11] the values of ($B_{ij}, i = j = 1, 2, \ldots, 6$) were determined by matching exact solutions to pure bending and the values of $\{K_{16}, K_{17}, K_{18}\}$ were determined by matching exact solutions to a higher-order hourglass modes. Determination of the coefficients

$$\{B_{77}, B_{78}, B_{79}, B_{88}, B_{89}, B_{99}\}, \tag{12}$$

corresponding to torsion solutions was less straight forward since it was impossible to satisfy all of the equations for pure torsion of a general rectangular parallelepiped. Motivated by the structure of the coefficients determined by exact integration of the tri-linear displacement field associated with the Bubnov–Galerkin procedure, the constitutive coefficients associated with (12) were proposed in the forms

$$B_{77} = (1-\nu^*)B\left[\frac{H_1^2 + H_2^2}{H_3^2}\right], \quad B_{78} = (1-\nu^*)B\left[\frac{H_1^2}{H_2 H_3}\right],$$

$$B_{79} = (1-\nu^*)B\left[\frac{H_2^2}{H_1 H_3}\right], \quad B_{88} = (1-\nu^*)B\left[\frac{H_1^2 + H_3^2}{H_2^2}\right],$$

$$B_{89} = (1-\nu^*)B\left[\frac{H_3^2}{H_1 H_2}\right], \quad B_{99} = (1-\nu^*)B\left[\frac{H_2^2 + H_3^2}{H_1^2}\right], \tag{13}$$

where the constant B is introduced here for convenience. Using these expressions it can be shown that the CPE predicts values of the torsional stiffnesses B_i for pure torsion of a rectangular parallelepiped in the forms

$$B_1 = \frac{T_1}{\omega_1} = \frac{\mu^* H_2^2 H_3^2}{3}\hat{b}\left(\frac{H_2}{H_3}\right),$$

$$B_2 = \frac{T_2}{\omega_2} = \frac{\mu^* H_1^2 H_3^2}{3}\hat{b}\left(\frac{H_1}{H_3}\right),$$

$$B_3 = \frac{T_3}{\omega_3} = \frac{\mu^* H_1^2 H_2^2}{3}\hat{b}\left(\frac{H_1}{H_2}\right), \tag{14}$$

where the function $\hat{b}(\xi)$ is given by

$$\hat{b}(\xi) = \frac{2B}{\xi + \frac{1}{\xi}}. \tag{15}$$

Comparison of the expressions (3) and (14) indicates that within the context of the theory of a CPE the exact function $b^*(\xi)$ in (4) for torsional stiffness is approximated by $\hat{b}(\xi)$ in (15). In [11] it was shown that the Bubnov–Galerkin value of the constant B in (15) is given by

$$B = \frac{1}{2} \text{ for Bubnov–Galerkin.} \tag{16}$$

Furthermore, it was noted that when the rectangular parallelepiped is a cube ($H_1 = H_2 = H_3$), which is the ideal aspect ratio for finite elements, then the approximate value of (15) equals the exact value of (4) when B is specified by

$$B = b^*(1) \approx 0.421732. \tag{17}$$

This value of B was specified for the CPE with a general reference geometry. Figure 1a plots the values of the exact function $b^*(\xi)$ in (4), denoted by (E), the values of $\hat{b}(\xi)$ with the original Cosserat specification (17), denoted by (O), and the values of $\hat{b}(\xi)$ with the Bubnov–Galerkin specification (16), denoted by (BG). Figure 1b plots the relative error E of these stiffnesses defined by

$$E = \frac{\hat{b}(\xi)}{b^*(\xi)} - 1. \tag{18}$$

From these figures it can be seen that, by design, the Cosserat solution is accurate for an ideal aspect ratio ($\xi = 1$) and predicts an error of (-15.6%) for very large aspect ratios (small values of ξ). In contrast, the Bubnov–Galerkin solution is accurate for large aspect ratios and predicts an error of 18.6% for an ideal aspect ratio.

Since the aspect ratios of finite elements are typically limited to be near ideal it was thought that the original Cosserat specification (17) would be more accurate than the Bubnov–Galerkin specification. However, it will be shown presently that, in spite of these results, it is better to specify the constant B by the Bubnov–Galerkin value (16). To this end, it

Fig. 1 Normalized torsional stiffnesses for the exact (E), the original CPE (O) and Bubnov–Galerkin (BG) solutions. **a** values of the functions $b^*(\xi)$ in (4) and $\hat{b}(\xi)$ in (15); and **b** relative errors (18)
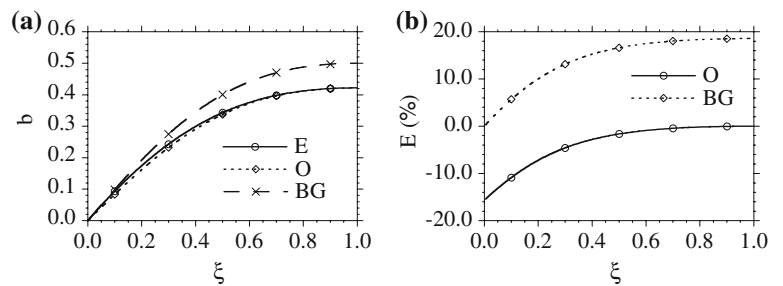
is recalled that within the context of the CPE theory, the position vector $\mathbf{X}^*$ and displacement vector $\mathbf{u}^*$ are related to the reference element director vectors $\mathbf{D}_i$ and the element director displacement vectors $\boldsymbol{\delta}_i$, such that

$$\mathbf{X}^* = \sum_{i=0}^{7} N^i(\theta^j)\mathbf{D}_i, \quad \mathbf{u}^* = \sum_{i=0}^{7} N^i(\theta^j)\boldsymbol{\delta}_i, \tag{19}$$

where the element region is defined by the convected coordinates θ^i

$$|\theta^1| \le \frac{H_1}{2}, |\theta^2| \le \frac{H_2}{2}, |\theta^3| \le \frac{H_3}{2}, \tag{20}$$

and the shape functions N^i are specified by the tri-linear forms

$$N^0 = 1, \quad N^i = \theta^i \ (i = 1, 2, 3), \quad N^4 = \theta^1\theta^2, \quad N^5 = \theta^1\theta^3,$$
$$N^6 = \theta^2\theta^3, N^7 = \theta^1\theta^2\theta^3. \tag{21}$$

For a rectangular parallelepiped the reference directors can be specified so that

$$\mathbf{D}_i = \mathbf{e}_i \ (i = 1, 2, 3), \quad \mathbf{D}_i = 0 \ (i = 4, 5, 6, 7). \tag{22}$$

Moreover, the value of $\mathbf{D}_0$ and the functional forms of the coordinates X_i associated with the specification (7) can be determined by equating (1) and (19) to deduce that

$$\mathbf{D}_0 = \bar{\mathbf{X}}^*, \quad X_i = (\bar{X}_i + \theta^i) \ (i = 1, 2, 3). \tag{23}$$

Thus, the displacement field associated with the simple torsion-like solution (8) [with $\omega_1 = \omega_2 = 0$] can be expressed in terms of the convected coordinates by

$$\mathbf{u}^* = -\omega_3(\bar{X}_2 + \theta^2)(\bar{X}_3 + \theta^3)\mathbf{e}_1 + \omega_3(\bar{X}_1 + \theta^1)(\bar{X}_3 + \theta^3)\mathbf{e}_2$$
$$+\omega_3\Phi_3(\bar{X}_1 + \theta^1)(\bar{X}_2 + \theta^2)\mathbf{e}_3. \tag{24}$$

An important difference between standard finite element methods and that used in the CPE theory is that the constitutive coefficients for the CPE are determined by matching exact solutions and not by integration over the element region. This means that although the displacement field (24) is a bilinear function of the convected coordinates, which is a special case of the tri-linear form (19), the equations of the CPE do not necessarily reproduce this solution exactly. More

specifically, it can be shown that the CPE will reproduce this exact simple solution only when the value of B is specified by the Bubnov–Galerkin value (16). The examples considered in the next section demonstrate that the simple torsion-like solutions (8) are basic solutions that should be reproduced exactly in order to improve the convergence properties for the more general pure torsion problem. Therefore, it is now suggested that the torsion coefficients (13) in the CPE theory be modified to use the value (16) instead of the original value (17). However, the other constitutive coefficients for the CPE remain those determined by the exact solutions of bending and higher order hourglassing modes, which are different from those determined by the Bubnov–Galerkin approach.

4 Examples

The objective of this section is to consider example problems which demonstrate that the convergence properties of the CPE for torsion problems are improved by using the value (16) instead of (17). In the following simulations, the full nonlinear equations [with $\omega_1 = \omega_2 = 0$] are solved even though for most of the calculations the magnitude of the twist

$$\omega_3 = 1 \times 10^{-3} \, \text{rad/m}, \tag{25}$$

is specified small enough that the response is essentially linear. Also, the three-dimensional material is characterized by the compressible Neo–Hookean strain energy function

$$2\rho_0^*\Sigma^* = K^*(J - 1)^2 + \mu^*(\alpha_1 - 3), \ J = \det(\mathbf{F}),$$
$$\alpha_1 = J^{-2/3}\mathbf{C} \cdot \mathbf{I}, \tag{26}$$

where $\mathbf{F}$ is the deformation gradient, $\mathbf{C} = \mathbf{F}^T\mathbf{F}$ is the right Cauchy–Green tensor, J is the dilatation, α_1 is a pure measure of distortion, ρ_0^* is the reference mass density, and the small deformation bulk modulus K^* and shear modulus μ^* are specified by

$$K^* = 1 \, \text{Gpa}, \quad \mu^* = 0.6 \, \text{Gpa}. \tag{27}$$

Results are presented for the modified CPE with the value (16) [denoted by (C)], for the original CPE with the value (17) [denoted by (O)], and for the enhanced strain element in FEAP [23] [denoted by (F)]. The element in FEAP is one of a class of 3-D brick finite elements that has been developed

based on enhanced strain/incompatible mode methods or reduced integration with hourglass control (e.g., [1,2,4,5, 12,13,19–21]) to model bending of thin structures. Calculations were also performed using the full integration element in FEAP and it was found that for pure torsion of a rectangular parallelepiped element, the response predicted by the full integration and enhanced strain elements are nearly the same. Consequently, the results for the full integration element are not recorded.

4.1 Pure torsion of a square cross-section (small deformations)

In this example the right-cylindrical region (1) is restricted to have a square cross-section with

$$L_1 = L_2 = L_3 = 1\,\text{m}, \tag{28}$$

and a twist ω_3 is applied in the $\mathbf{e}_3$ direction. Also, the case of pure torsion is considered so that the lateral surfaces ($X_1 = L_1/2$; $X_2 = L_2/2$) are traction free. Belytschko and Bindeman [1] proposed an assumed strain stabilization procedure for a brick element and considered a number of problems which included pure torsion. In particular, they simulated pure torsion by applying surface tractions to the cross-section. Here, an alternative approach is taken which specifies mixed-mixed boundary conditions on the cross-sections ($X_3 = 0$; $X_3 = L_3$). Specifically, the mesh is taken to be $\{n \times n \times 1\}$ and the nodes in the $X_3 = 0$ cross-section are fixed in the $\mathbf{e}_1 - \mathbf{e}_2$ plane and allowed to move freely in the $\mathbf{e}_3$ direction. Thus, the nodal displacement $\bar{\mathbf{u}}$ and $\bar{\mathbf{f}}$ force applied to a typical node in the cross-section ($X_3 = 0$) are restricted so that

$$\bar{\mathbf{u}} \cdot \mathbf{e}_1 = \bar{\mathbf{u}} \cdot \mathbf{e}_2 = 0, \bar{\mathbf{f}} \cdot \mathbf{e}_3 = 0 \text{ for } X_3 = 0. \tag{29}$$

Also, the nodal displacement and force applied to a typical node in the cross-section ($X_3 = L_3$) are restricted so that

$$\bar{\mathbf{u}} \cdot \mathbf{e}_1 = -\omega_3 L_3 X_2, \bar{\mathbf{u}} \cdot \mathbf{e}_2 = \omega_3 L_3 X_1,$$
$$\bar{\mathbf{f}} \cdot \mathbf{e}_3 = 0 \quad \text{for } X_3 = L_3. \tag{30}$$

In addition, one of the nodes in the cross-section ($X_3 = 0$) is prevented from moving in the $\mathbf{e}_3$ direction to eliminate rigid body translation.

Figure 2 shows the convergence of the error E of the torsional stiffness in (18) for the mesh $\{n \times n \times 1\}$, with the exact value of $b^*(1)$ given by (17). By design the original CPE (O) predicts zero error when the cross-section is modeled by a single element (n=1). It also predicts slightly better convergence than the modified form (C), which for this problem yields the same results as FEAP (F). This is consistent with the statement in [1] that "It is a simple matter to reduce the element stiffness in the warping mode so the one element
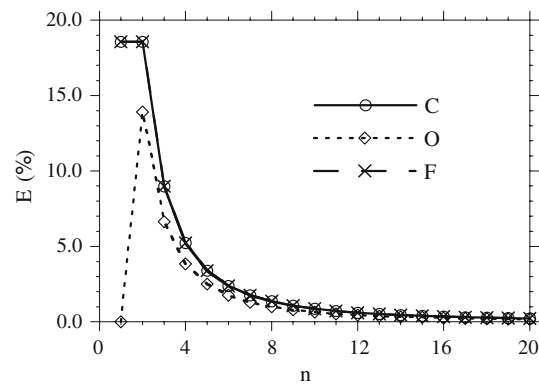

Fig. 2 Pure torsion of a square cross-section. Convergence of the error in the torsional stiffness predicted by the modified CPE (*C*), the original CPE (*O*) and FEAP (*F*) for the mesh $\{n \times n \times 1\}$

mesh has very accurate torsional stiffness ...; however, the more refined meshes will show little improvement...".

4.2 A rectangular cross-section (small deformations)

The second simulation considers a rectangular cross-section with aspect ratio ($L_2/L_1 = 5$) specified by

$$L_1 = 0.2\,\text{m}, \quad L_2 = L_3 = 1\,\text{m}. \tag{31}$$

For this cross-section the exact value of b^* is given by

$$b^*(0.2) \approx 0.174790. \tag{32}$$

Figure 3 shows the convergence properties for four different meshes. Convergence associated with the patch test is considered by the meshes Fig. 3a, b. Specifically, refinement is made in both the $\mathbf{e}_1$ and $\mathbf{e}_2$ directions with the mesh $\{n \times n \times 1\}$ preserving the aspect ratio ($H_2/H_1 = 5$) and with the mesh $\{n \times 5n \times 1\}$ preserving an ideal aspect ratio ($H_2/H_1 = 1$). Except for the point n=1 in Fig. 3a, b it can be seen that the original CPE (O) predicts slightly better convergence than the modified CPE (C) or FEAP (F). However, when the mesh is only refined in the $\mathbf{e}_2$ direction like $\{1 \times n \times 1\}$ in Fig. 3c and $\{2 \times n \times 1\}$ in Fig. 3d it can be seen that the modified CPE (C) and FEAP (F) continue to converge to the exact solution whereas the original CPE (O) converges to a solution that predicts an unphysical weaker torsional stiffness. These results clearly indicate that the displacement field in the simple torsion-like solution (8) is truly representative of the displacement field in elements during mesh refinement and that the convergence properties of the CPE can be significantly improved. Thus, it is important for an element formulation to produce a good approximation of the simple torsion-like solution.

Fig. 3 Pure torsion of a
rectangular cross-section with
aspect ratio $L_2/L_1 = 5$.
Convergence of the error in the
torsional stiffness predicted by
the modified CPE (C), the
original CPE (O) and FEAP (F)
for the meshes: **a** $\{n \times n \times 1\}$;
b $\{n \times 5n \times 1\}$; **c** $\{1 \times n \times 1\}$
and **d** $\{2 \times n \times 1\}$
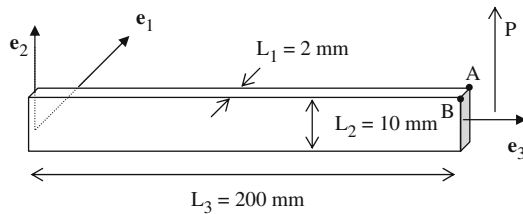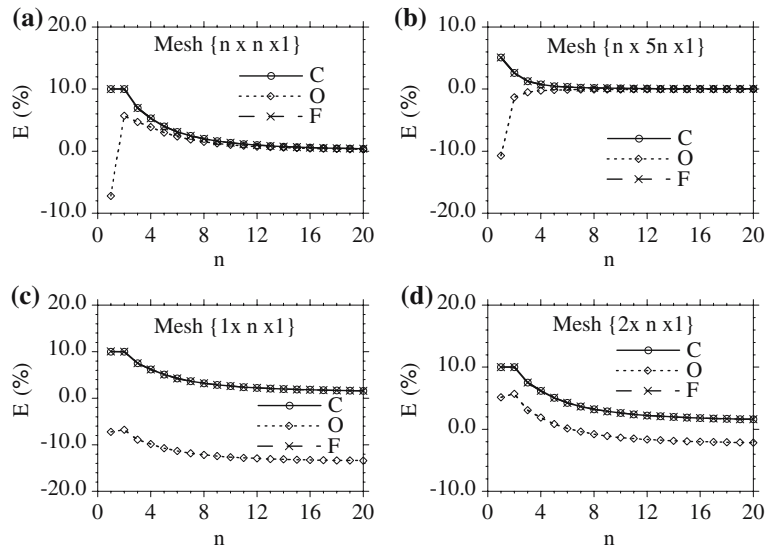
Fig. 4 Sketch of a thin cantilever beam subjected to a shear force P

4.3 Lateral torsional buckling (large deformations)

Figure 4 shows a sketch of a thin cantilever beam with a rect-
angular cross-section with aspect ratio ($L_2/L_1 = 5$) that is
specified by

$$L_1 = 2\,\text{mm}, \quad L_2 = 10\,\text{mm}, \, L_3 = 200\,\text{mm}. \tag{33}$$

The beam is clamped at its end $X_3 = 0$ with all nodes being
fixed and it is subjected to a shear force P that acts in the
constant $\mathbf{e}_2$ direction at its end $X_3 = L_3$. Specifically, the
nodal forces at this end are specified to be constant and are
determined by a uniform shear stress applied to the cross-sec-
tion. It is well known that lateral torsional buckling occurs at
a critical value of the load P for this beam with a rectangu-
lar cross-section. In order to plot the nonlinear post-buckling
response of the beam it is convenient to consider the displace-
ments $\mathbf{u}_A$ and $\mathbf{u}_B$ of the corners (A,B) of the cross-section
shown in Fig. 4 and define the average $\boldsymbol{\Sigma}_{\mathbf{u}}$ and difference $\boldsymbol{\Delta}_{\mathbf{u}}$
of these displacements by the expressions

$$\boldsymbol{\Sigma}_{\mathbf{u}} = \frac{1}{2}(\mathbf{u}_A + \mathbf{u}_B), \quad \boldsymbol{\Delta}_{\mathbf{u}} = \mathbf{u}_A - \mathbf{u}_B. \tag{34}$$

Also, it is convenient to introduce a small imperfection, such
that the beam is twisted in its stress-free reference config-
uration with the cross-sections X_3 being displaced relative
to the perfect beam by the displacement field (24) and the

specification

$$\omega_3 = 5 \times 10^{-6}\,\text{rad/mm}, \quad \Phi_3 = 0. \tag{35}$$

In this example the beam is subjected to shear and bending
before buckling and then combined shear, bending, extension
and torsion in the post-buckled state. The predictions of the
modified CPE for the most refined mesh $\{4 \times 20 \times 80\}$ are
considered to be exact and are denoted by (CE). Figure 5
shows the nonlinear response for three meshes with differ-
ent number of elements in the cross-sections together with
the exact solution. Specifically, the mesh for Fig. 5a, b is
$\{1 \times 1 \times 40\}$, that for Fig. 5c, d is $\{1 \times 5 \times 40\}$, and that for
Fig. 5e, f is $\{1 \times 10 \times 40\}$. In order to explore the convergence
properties of the solutions it is convenient to define the errors
E_Σ and E_Δ

$$E_\Sigma = \frac{\Sigma_{u2}}{\Sigma_{u2}^*} - 1, \quad E_\Delta = \frac{\Delta_{u2}}{\Delta_{u2}^*} - 1, \tag{36}$$

where Σ_{u2} and Δ_{u2} are the components of Σ_u and Δ_u in
the $\mathbf{e}_2$ direction for any calculation and Σ_{u2}^* and Δ_{u2}^* are the
values predicted by the most refined mesh $\{4 \times 20 \times 80\}$ of
the modified CPE for a load P greater than the buckling load

$$\Sigma_{u2}^* = 36.372\,\text{mm}, \quad \Delta_{u2}^* = 0.6980\,\text{mm}, \, P = 1.5\,N. \tag{37}$$

Figure 6 show convergence of these errors for two meshes
$\{1 \times 5n \times 40\}$ and $\{n \times 5n \times 40\}$.

From Fig. 5 it can be seen that the bending response is
captured accurately until the onset of buckling by all of the
elements even when there is no mesh refinement in the thin
$\mathbf{e}_1$ direction. However, the prediction of the buckling load
is very sensitive to the prediction of the torsional stiffness,
which is predicted more accurately by the modified CPE
(C) than by the original CPE (O). Also, from Fig. 6a, b it
can be seen that the original CPE (O) does not converge to
the correct solution when the mesh is refined only in the $\mathbf{e}_2$
direction.

Fig. 5 Post-buckling curves for a thin cantilever beam subjected to a shear force P for three meshes
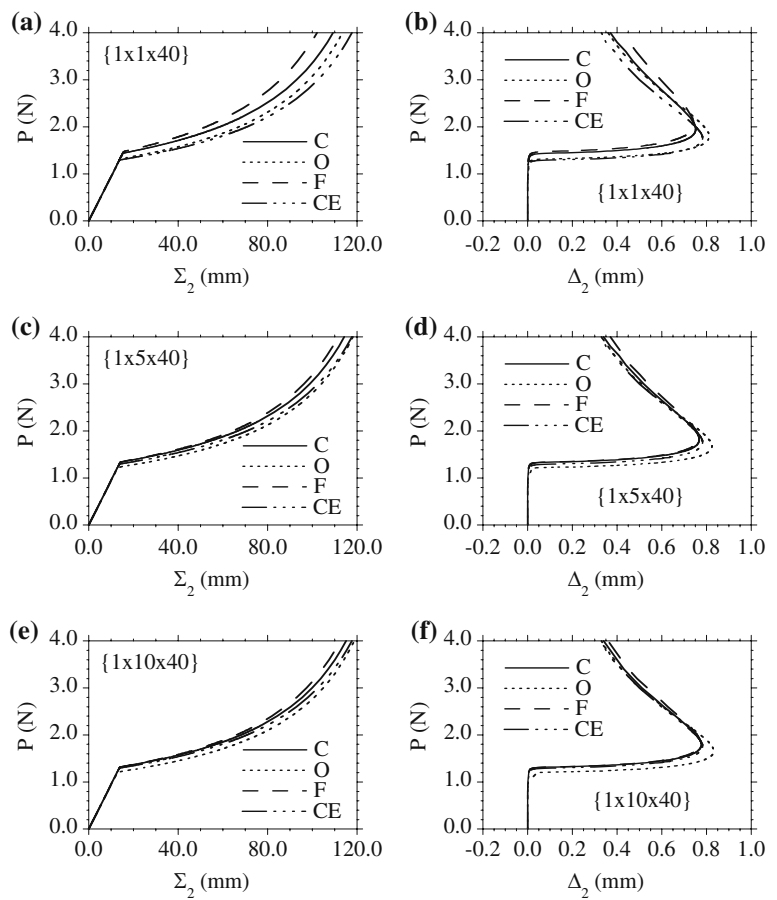
Fig. 6 Convergence of the errors E_Σ and E_Δ in (36) for two meshes: (**a**, **b**) $\{1 \times 5n \times 40\}$, and (**c**, **d**) $\{n \times 5n \times 20n\}$ with $P = 1.5\,\text{N}$
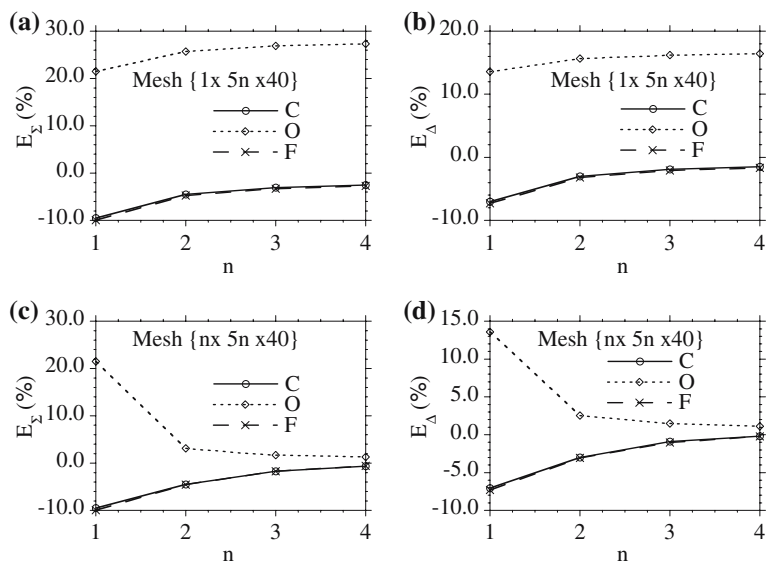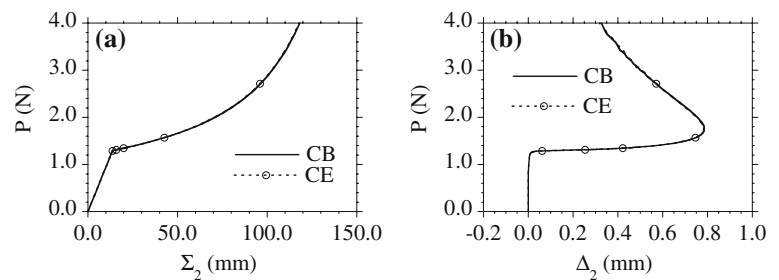

4.4 A beam element

Using the CPE approach it is not possible to predict all three exact torsional stiffnesses associated with a general parallelepiped. However, it is possible to use the 3-D brick CPE as a beam element by predetermining the axis of the beam as say $\mathbf{e}_3$ and then specifying the value of B in (15) by the exact

value B^* associated with the cross-section with dimensions $\{H_1, H_2\}$

$$B^* = \frac{1}{2}\left(\xi + \frac{1}{\xi}\right) b^*(\xi), \xi = \frac{H_1}{H_2}. \tag{38}$$

Figure 7 shows that the predictions of this beam element (CB) for the mesh $\{1 \times 1 \times 80\}$ and those of the modified CPE

Fig. 7 Post-buckling curves for
a thin cantilever beam subjected
to a shear force P modeled by
the beam CPE element (CB)
with the mesh {1 × 1 × 80} and
by the modified CPE (CE) with
the most refined mesh
{4 × 20 × 80}

(C) with the most refined mesh {4 × 20 × 80} are indistinguishable even though only one beam element is used in the cross-section. This emphasizes the importance of accurately modeling the torsional stiffness for this buckling problem.

5 Conclusions

The numerical solution of pure torsion of a right cylindrical bar with rectangular cross-section has been reexamined and an exact simple torsion-like solution has been identified which produces a good approximation of the deformation field in typical interior elements in the mesh for pure torsion. Modified torsional coefficients for a 3-D brick CPE are proposed which cause the CPE theory to reproduce the simple torsion-like solution exactly. Examples of small deformation pure torsion and large deformation lateral torsional buckling of a cantilever beam demonstrate that the convergence properties of the modified CPE are significantly improved relative to those of the original CPE. Also, constitutive coefficients for the 3-D brick CPE have been proposed to obtain a beam element which predicts accurate response for lateral torsional buckling with only one element modeling the rectangular cross-section.

Attention has been limited to isotropic material response because no functional form is yet available for the strain energy of inhomogeneous deformations of a CPE modeling an anisotropic material.

References

1. Belytschko T, Bindeman LP (1993) Assumed strain stabilization of the eight node hexahedral element. Comp Meth Appl Mech Eng 105:225–260
2. Belytschko T, Ong JSJ, Liu WK, Kennedy JM (1984) Hourglass control in linear and nonlinear problems. Comp Meth Appl Mech Eng 43:251–276
3. Boerner EFI, Loehnert S, Wriggers P (2007) A new finite element based on the theory of a Cosserat point—extension to initially distorted elements for 2D plane strain. Int J Numer Methods Eng (in press)
4. Bonet J, Bhargava P (1995) A uniform deformation gradient hexahedron element with artificial hourglass control. Int J Numer Methods Eng 38:2809–2828
5. Hutter R, Hora P, Niederer P (2000) Total hourglass control for hyperelastic materials. Comp Meth Appl Mech Eng 189:991–1010
6. Jabareen M, Rubin MB (2007) Hyperelasticity and physical shear buckling of a block predicted by the Cosserat point element compared with inelasticity and hourglassing predicted by other element formulations. Comput Mech 40:447–459
7. Jabareen M, Rubin MB (2007) An improved 3-D Cosserat brick element for irregular shaped elements. Comput Mech (in press)
8. Klepach D, Rubin MB (2007) Influence of membrane stresses on postbuckling of rectangular plates using a nonlinear elastic 3-D Cosserat brick element. Comput Mech 39:729–740
9. Lekhnitskii SG (1963) Theory of elasticity of an anisotropic elastic body. Holden-Day, San Francisco
10. Loehnert S, Boerner EFI, Rubin MB, Wriggers P (2005) Response of a nonlinear elastic general Cosserat brick element in simulations typically exhibiting locking and hourglassing. Comput Mech 36:255–265
11. Nadler B, Rubin MB (2003) A new 3-D finite element for nonlinear elasticity using the theory of a Cosserat point. Int J Solids Struct 40:4585–4614
12. Reese S, Wriggers P (1996) Finite element calculation of the stability behaviour of hyperelastic solids with the enhanced strain methods. Zeitschrift Angewandte Math Mech 76:415–416
13. Reese S, Wriggers P, Reddy BD (2000) A new locking free brick element technique for large deformation problems in elasticity. Comput Struct 75:291–304
14. Rubin MB (1985) On the theory of a Cosserat point and its application to the numerical solution of continuum problems. J Appl Mech 52:368–372
15. Rubin MB (1985) On the numerical solution of one-dimensional continuum problems using the theory of a Cosserat point. J Appl Mech 52:373–378
16. Rubin MB (1995) Numerical solution of two- and three-dimensional thermomechanical problems using the theory of a Cosserat point. J Math Phys (ZAMP) 46, Special Issue, S308–S334. In: Casey J, Crochet MJ (ed) Theoretical, experimental, and numerical contributions to the mechanics of fluids and solids. Birkhauser Verlag, Basel
17. Rubin MB (2000) Cosserat theories: shells, rods and points. Solid mechanics and its applications, vol 79. Kluwer, The Netherlands
18. Rubin MB (2005) Numerical solution of axisymmetric nonlinear elastic problems including shells using the theory of a Cosserat point. Comput Mech 36:266–288
19. Simo JC, Armero F (1992) Geometrically non-linear enhanced strain mixed methods and the method of incompatible modes. Int J Numer Meth Eng 33:1413–1449

20. Simo JC, Rifai MS (1990) A class of mixed assumed strain methods and the method of incompatible modes. Int J Numer Meth Eng 29:1595–1638
21. Simo JC, Armero F, Taylor RL (1993) Improved versions of assumed enhanced strain tri-linear elements for 3D finite deformation problems. Comp Meth Appl Mech Eng 110:359–386
22. Sokolnikoff IS (1964) Mathematical theory of elasticity. McGraw-Hill, New York
23. Taylor RL (2005) FEAP—a finite element analysis program, version 7.5. University of California, Berkeley